A surface-enhanced hyper-Raman and surface-enhanced Raman scattering study of *trans*-1,2-bis(4-pyridyl)ethylene adsorbed onto silver film over nanosphere electrodes. Vibrational assignments: Experiment and theory

Wen-hui Yang, John Hulteen, George C. Schatz,[a] and Richard P. Van Duyne[a]
Department of Chemistry, Northwestern University, Evanston, Illinois 60208-3113

(Received 10 October 1995; accepted 15 December 1995)

We present theoretical and experimental studies of the infrared (IR) spectroscopy, normal Raman spectroscopy (NRS), surface-enhanced Raman spectroscopy (SERS), and surface-enhanced hyper-Raman (SEHRS) spectroscopy of *trans*-1,2-bis(4-pyridyl)ethylene (BPE). This centrosymmetric molecule is expected to have no common Raman and hyper-Raman lines provided that it is not strongly perturbed by adsorption on the surface. The measured SERS spectrum, obtained under electrochemical conditions on Ag film over nanosphere (AgFON) electrodes, shows a well defined C=C stretch band that is not seen in the SEHRS spectrum, but many of the other bands overlap closely. We use *ab initio* calculations for isolated BPE to assign the spectra, and find excellent agreement between the calculated and measured IR and SERS spectra, and good agreement between the calculated and measured SEHRS spectrum. We find that the apparently overlapping IR, SERS, and SEHRS bands are in fact due to modes that have similar vibrational characteristics but different symmetry. Our results indicate that SEHRS spectra are consistent with the expected (three photon) selection rules and intensities. This rules out an alternative mechanism in which the observed spectrum arises from surface second harmonic generation (SHG) followed by SERS excited at the second harmonic frequency. © *1996 American Institute of Physics.* [S0021-9606(96)03111-3]

I. INTRODUCTION

Hyper-Raman spectroscopy (HRS) is a nonlinear Raman technique in which the emitted photon is shifted relative to the second harmonic of the incident radiation (i.e., $\omega=2\omega_0-\Delta\omega$, where $\Delta\omega$ is the vibrational frequency). Since three photons are involved, the selection rules for HRS are very different than for normal Raman spectroscopy (NRS), and in particular for a centrosymmetric molecule, there should be no common Raman and hyper-Raman transitions. Instead, all infrared (IR) active modes are also allowed in the hyper-Raman spectrum. In addition, there are some modes such as the A_u vibrations in the D_{2h} point group that are silent in both NRS and IR but active in HRS. Because of the high fields that are usually required to observe hyper-Raman spectra, there have been very few HRS studies in gases or liquids.[1] However, in the past few years, interest in HRS has grown[2–5] because of the relative ease of measurements in environments where surface-enhanced Raman spectroscopy (SERS) is possible. Surface-enhanced HRS (SEHRS) was originally demonstrated by Chang.[2] More recent studies by Van Duyne, Nie, Lipscomb, and others[3–5] have reported high quality SEHR spectra for pyridine and several other molecules adsorbed onto silver electrode and colloid surfaces.

One of the most interesting conclusions from the pyridine studies[3] is that the SEHRS enhancement factor is approximately 10^{12}. This value, which has recently been independently confirmed,[5(c)] is much larger than would be expected based on enhancement factors for SERS and second harmonic generation (SHG) (Ref. 6) from the electromagnetic mechanism[7] (wherein the electromagnetic field is amplified near the metal surface due to surface plasmon excitation). This suggests that other enhancement effects may play a stronger role in SEHRS than in SERS. This could provide important clues for determining which of the possible nonelectromagnetic mechanisms is involved in SERS and SEHRS. However, an important assumption in this analysis has been that the spectra arising at $2\omega_0-\Delta\omega$ are due to SEHRS and not some other process. Perhaps the most obvious alternative is a two step process in which first SHG at the surface produces photons at $2\omega_0$ and then these photons scatter off the adsorbed molecules in an ordinary SERS process so that the final frequency is still $2\omega_0-\Delta\omega$.

A possible way to distinguish between these two mechanisms is to examine spectra of a molecule which is centrosymmetric, as the selection rules should distinguish whether the molecule is directly involved in the three photon process (SEHRS) or whether it sees just two photons (SERS). Actually, the inversion symmetry does not have to be rigorously preserved in the presence of an interface; we really only need the spectra to be imperceptibly different from those with rigorous symmetry conservation.

In this paper we consider this possibility using *trans*-1,2-bis(4-pyridyl)ethylene (which henceforth will be called BPE). Besides being centrosymmetric, this molecule is photostable and exhibits very intense SER and SEHR spectra using relatively modest laser powers {even enabling the observation of CW SEHRS [Ref. 8(a)]}, with lines that are well resolved. In addition, Hulteen *et al.*[8(b)] have studied the electrochemical potential dependence of SER and SEHR spectra

[a]Authors to whom correspondence should be addressed.

 0021-9606/96/104(11)/4313/11/$10.00

of BPE. They find that at applied potentials more negative that −0.7 V vs Ag/AgCl, most lines of the SEHR spectrum and all lines of the SER spectrum are not significantly perturbed by the electrode potential or by coadsorbates. Thus under these conditions, the strength of adsorption is weak and the perturbations in the spectra associated with adsorption on the surface are not important.

The primary goal of this study is to analyze the IR, NRS, SERS and especially the SEHRS of BPE to see if the spectra are consistent with the expected selection rules for a centrosymmetric molecule. In the process of doing this, we will attempt to assign many of the spectral lines, but we should emphasize that this work is not intended to be an exhaustive exercise in spectral analysis. The SER and SEHR spectra have been collected under electrochemical control, using an Ag film-over-nanosphere (AgFON) substrate. This substrate, which is produced by vapor deposition of silver onto a monolayer of polystyrene nanospheres that are coated onto a flat silver surface, provides controllable roughness on a size scale that is ideal for SERS and SEHRS experiments.[9]

One disadvantage of using BPE is that its spectra are relatively complex and have not been fully assigned. To circumvent this problem, we use *ab initio* calculations to make spectral assignments, including IR, NR, SER, and SEHR spectra. This sort of comparison between theory and experiment was used previously[10] in studies of SER and SEHR spectra of pyridine, and it was found that Hartree–Fock (HF) calculations using basis sets that include diffuse functions give spectra that match reasonably well with experiment. The application of the same approach to BPE is computationally challenging but doable, and the results, as we shall see, enable assignment of many of the lines in the spectra.

To summarize the rest of this manuscript, in Sec. II we describe the experimental measurements and present the IR, NR, SER, and SEHR spectra. The theoretical calculations and spectra are described in Sec. III, and the comparisons with experiment are discussed in Sec. IV. Section V summarizes our conclusions.

II. EXPERIMENT

A. Materials

trans-1,2-bis(4-pyridyl)ethylene (BPE) was purchased from Aldrich, recrystallized twice from methanol/water and sublimed. Water was obtained from a Millipore water filtration system, and KCl was purchased from Mallinckrodt. Ag (99.99%) was purchased from D. F. Goldsmith (Evanston, IL), and W vapor deposition boats were purchased from R. D. Mathis (Long Beach, CA). Polystyrene nanospheres, diameter=542±7 nm, with a terminal carboxyl functional group were purchased from IDC (Portland, OR) and were diluted 1:1 by volume with a solution of the surfactant Triton X-100 (Aldrich) and methanol (1:400 by volume) to promote a close-packing arrangement.

B. Spectroscopy

The infrared spectra were recorded using a BOMEM MB-Series FT-IR spectrometer. Spectra were obtained from KBr films with 64 scans at a resolution of 2 cm^{-1}.

The NR, SER, and SEHR spectra were recorded on an ACTON VM-505 (Acton, MA) single grating monochromator equipped with a Photometrics PM-512 CCD detector (Tucson, AZ). A Spectra Physics Series 3000 cw mode-locked Nd:YAG was used for $\lambda_{ex}=1064$ nm and 532 nm. A Physical Optics Co. (Torrance, CA) holographic edge filter was used for rejection of λ_{ex} in both NRS and SERS experiments, while Schott glass filter 59062 was used to reject λ_{ex} in SEHRS experiments. The angle of incidence of the laser excitation source was 45° with respect to the surface normal, and scattered light was collected parallel to the surface normal with f/1 optics. In all spectra, the laser source was spot-focused to ca. an 100 μm diam.

C. AgFON preparation

AgFON electrodes were prepared by spin coating a monolayer of the polystyrene nanospheres onto a polished Ag disk electrode (diameter=5 mm) on a spin coater designed in-house. The Ag disk electrode consisted of an Ag rod sealed with an epoxy (Torr Seal, Varian) into a Teflon frame. The electrode was then placed in a modified Consolidated Vacuum Corporation vapor deposition system with a base pressure of 10^{-7} Torr. A 200 nm Ag film was grown over the nanospheres by thermal vapor deposition from a W boat at a rate of 0.3–0.4 nm s^{-1}. The electrode temperature remained <50 °C, and the chamber pressure was always $<10^{-6}$ Torr during the deposition. Mass thickness was measured with an in-house designed quartz-crystal microbalance calibrated by both cyclic voltammetry and STM. The spectroelectrochemical cell was designed in-house and all reported potentials are with respect to an Ag/AgCl reference electrode.[9]

D. Results

Figures 1–4 present the measured spectra [part (B) of each figure], along with theoretical results [part (A)] that are described below. The spectra include IR (Fig. 1), NRS (Fig. 2), SERS (Fig. 3), and SEHRS (Fig. 4). Only frequencies between 400 and 1700 cm^{-1} are shown. Some additional details associated with the measurements are given in the figure captions. We will defer interpretation of the spectra until Sec. IV.

III. THEORY

A. Basic intensity expressions

To calculate Raman and hyper-Raman intensities (either on or off the surface), we use general expressions from Ref. 1 which relate these intensities to the appropriate components of the molecular polarizability and hyperpolarizability derivatives. IR intensities were calculated at the same time from dipole derivatives.

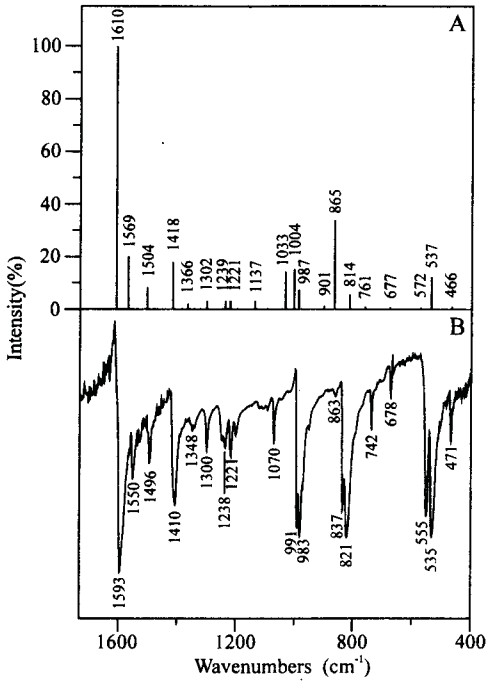

FIG. 1. IR spectrum of BPE. (a) shows the theoretical result, while (b) shows the observed result in a KBr film, 64 scans, 2 cm^{-1} resolution.

Let us consider the experimental geometry wherein scattering is observed at 90° relative to the incident beam direction, and polarization of the scattered beam is not resolved. The resulting expression for the orientation averaged normal Raman spectrum (NRS) is given by[10,11]

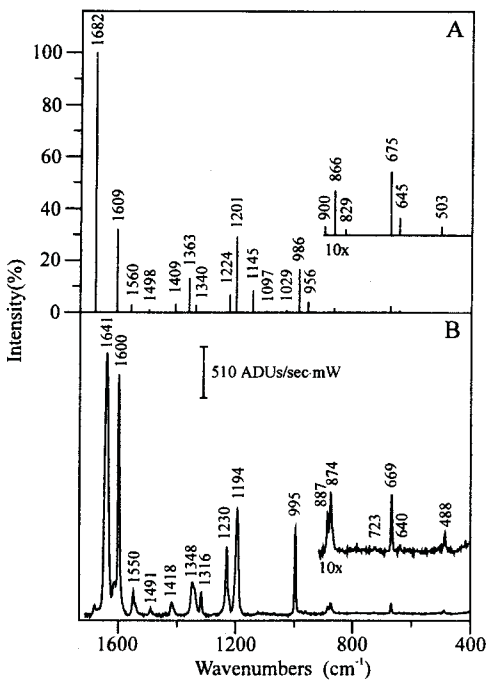

FIG. 2. NR spectrum of BPE. (a) shows the calculated result, while (b) shows result for solid BPE with 30 mW of λ_{ex}=532 nm, 1 s integration.

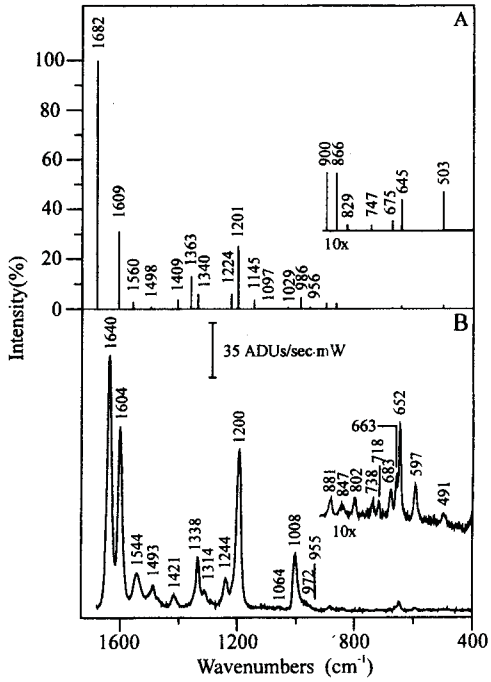

FIG. 3. SER spectrum of BPE. (a) shows the calculated result, while (b) shows the measured spectrum of 0.4 mM BPE on a AgFON electrode where [Cl$^-$]=0.1 M at a fixed potential E=−0.7 V with 10 mW of λ_{ex}=532 nm, 30 s integration.

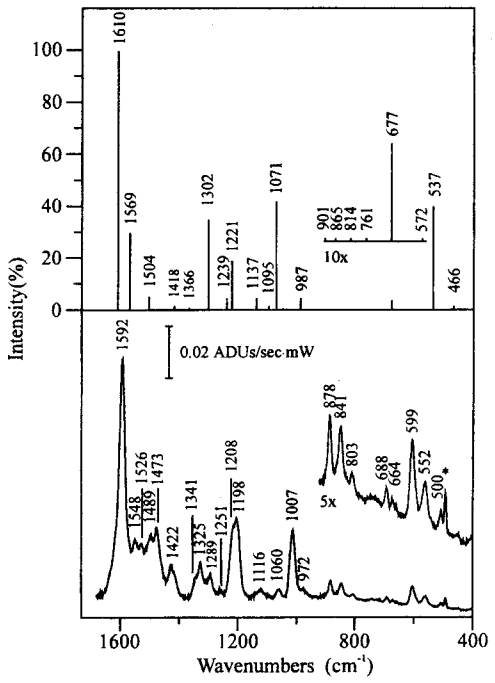

FIG. 4. SEHR spectrum of BPE. (a) shows the calculated result, while (b) shows the measured SEHRS spectrum of 0.4 mM BPE on an AgFON electrode where [Cl$^-$]=0.1 M at a fixed potential E=−0.7 V with 1.0 W of λ_{ex}=1064 nm, 300 s integration. The (*) indicates a Hg line from stray room lights.

$$I_R=\frac{\omega^4}{c^4} I_0(\langle \tilde{\alpha}'^2_{ii}\rangle+\langle \tilde{\alpha}'^2_{ij}\rangle)=\frac{\omega^4}{c^4} I_0\left(\bar{\alpha}'^2+\frac{7}{45}\gamma'^2\right), \quad (1)$$

where I_0 is the incident radiation intensity, ω is the scattered frequency ($\omega=\omega_0-\Delta\omega$), $\tilde{\alpha}'_{ij}$ denotes the i,jth element relative to a space-fixed coordinate system (signified by the tilda ˜) of the polarizability derivative (prime denotes derivative) with respect to a vibrational normal coordinate. The brackets signify that an orientation average needs to be done, $\bar{\alpha}'$ is the trace of the polarizability derivative, and γ' is the derivative of the anisotropy.[11]

The corresponding intensity expression for hyper-Raman scattering (HRS) is[10–14]

$$I_{\mathrm{HR}}=\frac{8\pi\omega^4}{c^5} I_0^2 \sum_{ij} \langle \tilde{\beta}'^2_{ijj}(\omega,Q)\rangle, \quad (2)$$

where

$$\begin{aligned}\sum_{ij}\langle \tilde{\beta}'^2_{ijj}(\omega,Q)\rangle=&\langle \tilde{\beta}'^2_{iii}\rangle+\langle \tilde{\beta}'^2_{ijj}\rangle=\frac{6}{35}\sum_i \beta'^2_{iii}+\frac{8}{105}\sum_{i\neq j}\beta'_{iii}\beta'_{ijj}+\frac{2}{35}\sum_{i\neq j}\beta'_{iii}\beta'_{jji}+\frac{4}{21}\sum_{i\neq j}\beta'^2_{ijj}+\frac{4}{35}\sum_{i\neq j}\beta'^2_{ijj}\\&+\frac{2}{35}\sum_{i\neq j\neq k}\beta'_{ijj}\beta'_{jkk}+\frac{4}{105}\sum_{i\neq j\neq k}\beta'_{ijj}\beta'_{ikk}+\frac{2}{105}\sum_{i\neq j\neq k}\beta'_{iik}\beta'_{jjk}+\frac{2}{105}\sum_{i\neq j\neq k}\beta'_{iij}\beta'_{jkk}\\&+\frac{2}{21}\sum_{i\neq j\neq k}\beta'^2_{ijk}+\frac{4}{105}\sum_{i\neq j\neq k}\beta'_{ijk}\beta'_{jki}. \quad (3)\end{aligned}$$

Here ω is again the scattered frequency ($\omega=2\omega_0-\Delta\omega$), and $\tilde{\beta}'_{ijk}$ is the ijkth space-fixed element of the hyperpolarizability derivative. Here we use the symbol β' without the tilde to denote the molecule-fixed components of the hyperpolarizability derivative.

To estimate SERS and SEHRS intensities, we assume that the long axis of the BPE molecule is perpendicular to the surface. This result appears to be consistent with experimental observation, as we will show later. Since the field near the surface is dominated by its normal component, only the components of α' and β' perpendicular to the surface contribute to spectra. Denoting this perpendicular direction as z, then the intensities are proportional to α'^2_{zz} and β'^2_{zzz}. In separate calculations, we have also considered the possibility that the long axis of the molecule is oriented in directions other than along the z axis. The appropriate intensity expressions are given by Yang and Schatz.[9] We will examine the results to determine the sensitivity of the spectra to orientation.

B. Computations

There are two components to the calculation of the infrared, Raman and hyper-Raman intensities; (1) calculation of the normal coordinates, and (2) calculation of the derivative of the dipole moment, polarizability, and hyperpolarizability with respect to these normal coordinates. We have used HF calculations based on GAUSSIAN 92 to calculate the normal coordinates after full optimization of the molecular geometry. An important conclusion of Ref. 9 is that it is crucial to include diffuse functions in the basis functions to calculate hyper-Raman intensities. Since the molecule we consider here, BPE, consists of 24 atoms, the appropriate basis set needs to be chosen with care if the calculations are to be feasible. The basis set that we have chosen, 6-31+G, strikes a reasonable compromise between the need for diffuse functions, and feasibility of the calculations.

In calculating the molecular dipole moments, polarizabilities, and hyperpolarizabilities of pyridine, it was determined in Ref. 9 that HF calculations based on GAUSSIAN are preferred relative to CIS (singles CI) based on the INDO program ZINDO, especially with respect to the out-of-plane modes. Although GAUSSIAN determines only the zero frequency polarizabilities and hyperpolarizabilities, the error due to frequency dependence is minor for pyridine at frequencies relevant to the experiments. For BPE we have used GAUSSIAN 92 (Ref. 15) for all calculations.

As in our earlier work, we use finite differencing to determine the hyperpolarizability derivatives. As a check on this, we have verified that finite differencing applied to the dipole moment and polarizability yield results in agreement with the analytical results provided by GAUSSIAN 92.

C. Calculated intensities

Table I presents the calculated vibrational frequencies and normalized bulk IR, Raman, and hyper-Raman intensities, along with experimental assignments that we discuss later. BPE has 66 modes, including 23 of A_g symmetry (in C_{2h} symmetry) which are Raman allowed, 22 of B_u symmetry (IR and hyper-Raman allowed), 10 of B_g symmetry (Raman allowed), and 11 of A_u symmetry (IR and hyper-Raman allowed). Note that the A_g and B_u modes are in-plane while the others are out-of-plane. There are 10 C–H stretch modes near 3000 cm^{-1}, 5 each of A_g and B_u symmetry. These have been included in the table, but we will ignore them in the discussion as they are weak in the SERS and SEHRS spectra. We have also omitted six modes with frequencies below 250

TABLE I. Vibrational spectra of BPE.

Symmetry		Calculated frequencies (cm^{-1})	Raman (bulk) intensity	Experimental NRS (cm^{-1})	Experimental SERS (cm^{-1})
A_g	17	280	0.6		320
	16	645	0.6	640	652
	15	675	2.4	669	663
	14	866	1.7	874	847
	13	986	16.7	995	1008
	12	1071	0.3		1064
	11	1097	0.6		
	10	1145	8.6	1194	1200
	9	1201	29.3	1194	1200
	8	1224	7.0	1230	1244
	7	1340	2.8	1316	1314
	6	1363	13.1	1348	1338
	5	1409	3.3	1418	1421
	4	1498	1.0	1491	1493
	3	1560	2.9	1550	1544
	2	1609	33.2	1600	1604
	1	1682	100.0	1641	1640
		3018	7.9		
		3034	7.8		
		3049	2.9		
		3061	25.0		
		3069	8.8		
B_g	8	409	<0.1		400
	7	503	0.3	488	491
	6	747	<0.1	723	738
	5	829	0.2		802
	4	900	0.3	887	881
	3	956	4.2		955,972
	2	1029	0.8		1064
	1	1047	<0.1		

Symmetry		Calculated frequencies (cm^{-1})	Calculated intensity IR (bulk)	Calculated hyper-Raman (bulk)	Experimental IR (bulk)	Experimental SEHRS
B_u	16	466	1.0	1.4	471	552
	15	537	12.2	42.9	535	599
	14	677	0.7	7.2	678	688
	13	814	5.6	<0.1	821	841
	12	987	7.4	8.5	983	972
	11	1071	0.2	46.6		1007
	10	1095	0.4	6.8		1116
	9	1137	3.1	24.7	1200	1198
	8	1221	3.2	21.5	1221	1208
	7	1239	3.1	11.7	1238	1289
	6	1302	3.1	37.1	1300	1325
	5	1366	2.1	2.7	1348	1341
	4	1418	18.0	5.4	1410	1422
	3	1504	8.3	10.9	1496	1489
	2	1569	20.2	41.4	1550	1548
	1	1610	100.0	100.0	1593	1593
		3012				
		3033				
		3049				
		3061				
		3069				
A_u	9	298	2.8	2.8		306
	8	408	<0.1	<0.1		385
	7	572	0.6	0.4	555	664
	6	761	0.9	1.1	742	803
	5	865	33.9	1.2	837	878
	4	901	1.3	0.2	863	
	3	1004	15.2	0.6	991	

TABLE I. (*Continued.*)

Symmetry	Calculated frequencies (cm^{-1})	Calculated intensity IR (bulk)	Calculated hyper-Raman (bulk)	Experimental IR (bulk)	Experimental SEHRS
2	1033	14.2	1.8	1070	1060
1	1047	0.4	0.1		

cm^{-1}, as such frequencies are not determined accurately in the measurements, and the calculated frequencies are probably strongly perturbed by anharmonicity. This leaves us with 17 A_g, 16 B_u, 8 B_g, and 9 A_u modes that are of primary interest.

We have introduced a numbering system for the modes to facilitate the later discussion. Excluding, the 10 C–H stretch modes, the modes are numbered from largest to smallest frequency within each irreducible representation. This means that the mode labeled $1(A_g)$ is the 1682 cm^{-1} mode in the table. Note that the frequencies from the HF calculations have been scaled by 0.9, which is a typical correction factor for HF frequencies.[16]

To facilitate comparison with experiment, we present stick spectra in Figs. 1–5 based on the calculations. Figures 1–4 are the IR, NR, SER, and SEHR spectra as noted above, while Fig. 5 is the bulk HR spectrum (for which there is no experimental measurement). To show the effect of orientation of the molecule relative to the surface, in Fig. 6 we present SER spectra for four different orientations; (a) 0° relative to the surface normal, i.e., with the C_2 axis perpendicular to the surface, (b) 30°, (c) 60°, and (d) 90°. Figure 7 presents the corresponding SEHRS spectra for different orientations.

Figures 8 and 9 show the normal coordinate displacements for selected modes. These include modes 1, 2, 3, 6, 9, and 13 of A_g symmetry in Fig. 8, and modes 1, 2, 6, 8, 11, and 12 of B_u symmetry in Fig. 9. Note that most of the modes come in pairs, such as $2(A_g)$ and $1(B_u)$ [i.e., Figs. 8(b) and 9(a)]; $3(A_g)$ and $2(B_u)$ [i.e., Figs. 8(c) and 9(b)]. These modes have nearly the same frequency, and the same vibrations for each pyridine ring within a pair, with the A_g mode corresponding to the in-phase combination of the ring motions and the B_u mode the out-of-phase combination. Modes that involve significant motions of the ethylenic fragment do not always come in pairs. The best example of this mode $1(A_g)$. in Fig. 8(a), which corresponds to the C=C stretch of the ethylenic fragment. Generally we find that the modes labeled $k(A_g)$ are paired with $k-1(B_u)$ with $k=2,3,...$, and also the modes $k(B_g)$ are paired with $k(A_u)$ with $k=1,2,3,...$. An exception to this rule is that mode $8(A_g)$ is paired with $8(B_u)$, while $9(A_g)$ is paired with $7(B_u)$. The latter pair shows one of the largest splittings between pairs, in this case 38 cm^{-1}.

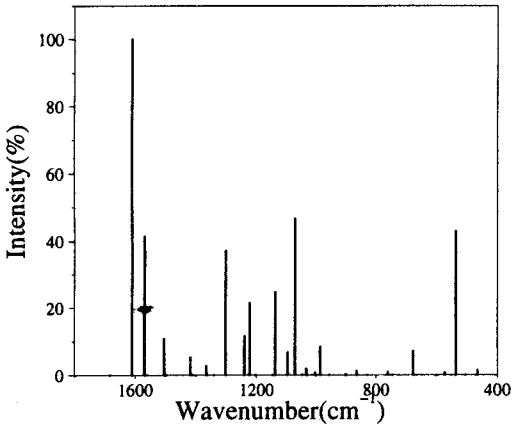

FIG. 5. Calculated bulk hyper-Raman spectrum of BPE.

IV. COMPARISON OF THEORY AND EXPERIMENT

A. IR spectra

Let us now discuss the IR results in Fig. 1 and Table I. The assignments in Table I have been made by inspection of

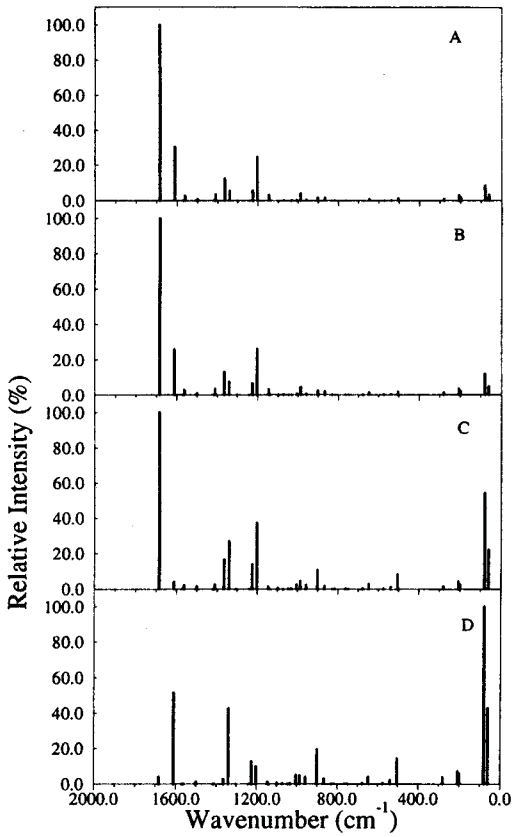

FIG. 6. Calculated SER spectrum of BPE for different orientations. The angles between the molecular axis and surface perpendicular are (a) 0, (b) 30, (c) 60, and (d) 90.

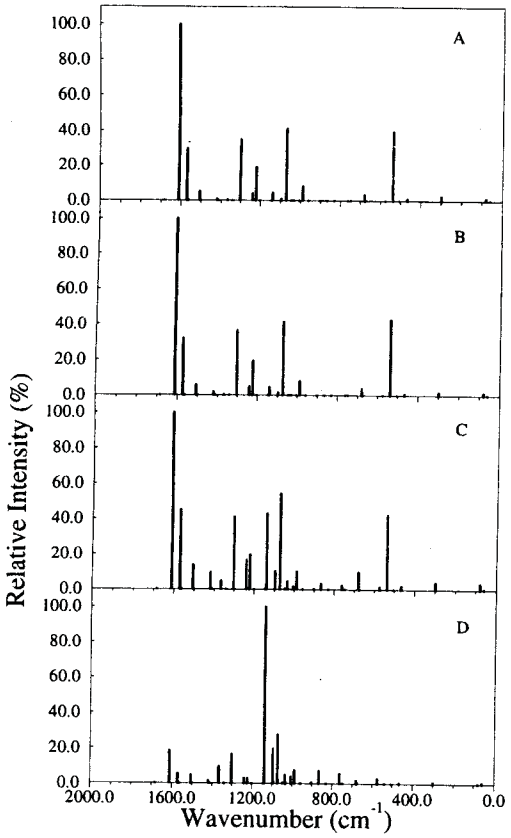

FIG. 7. Same as Fig. 6 but for SEHRS.

the frequencies and intensities in Fig. 1, and are reasonably straightforward for the most intense peaks, but are uncertain for many of the weak ones. The overall agreement between theory and experiment is quite reasonable for the level of calculation that we have done, with an average absolute deviation of 11 cm^{-1} for the B_u modes and 25 cm^{-1} for the A_u modes. The correspondence for the high frequency modes (>1300 cm^{-1}) is best, with no unexplained peaks in the data, and both intensities and frequencies in good agreement. The most intense IR mode is at an experimental frequency of 1593 cm^{-1}, and is a ring stretching mode which corresponds to the displacements shown in Fig. 9(a). The characteristics of some of the other modes in this region will be discussed later. Below 1300 cm^{-1} there are some places where the assignments are more ambiguous, such as near the group of peaks labeled 1221 cm^{-1} and 1238 cm^{-1} in the measured results (where a quartet appears in the measurements while only a doublet is predicted). Presumably these extra peaks are due to forbidden transitions associated with A_g modes that are found at approximately the same frequencies.

B. Normal and surface enhanced Raman spectra

First let us consider the NRS results in Fig. 2 and Table I. The comparisons between theory and experiment are found to be comparable in quality to the IR results, with excellent agreement for modes above 1300 cm^{-1}, and good for modes below, and an average absolute difference between theory and experiment of 14 cm^{-1} for the modes that have been assigned. The progression of A_g modes at 1682, 1609, 1560, 1498, 1409, 1363, and 1340 cm^{-1} (giving the calculated frequencies) is essentially in one-to-one correspondence with the measured NRS frequencies in Fig. 2, and also showing a good match in intensities. The most intense Raman peak is calculated to be at 1682 cm^{-1}, and corresponds to the ethylenic stretch [Fig. 8(a)]. Another intense mode is at 1609 cm^{-1}, corresponding to pyridine ring C=C stretch [Fig. 8(b)]. A third intense mode is at 1363 cm^{-1}, and corresponds to CH wag [Fig. 8(d)].

We assume that the modes at 1224, 1201, and 1145 cm^{-1} in the calculated spectrum have been grouped into two peaks (at 1230 cm^{-1} and 1194 cm^{-1}) in the measured NR spectrum. The peak at 1230 cm^{-1} is clearly a doublet, but it is not clear to us which two of the three calculated peaks belong to this doublet. The modes calculated at 1201 cm^{-1} and 1145 cm^{-1} have significant ethylenic C=C stretch character [Fig. 8(e) shows the 1201 cm^{-1} mode] while that at 1224 cm^{-1} involves C–H bending on the pyridine ring.

The strong peak at 995 cm^{-1} (NRS) corresponds to 986 cm^{-1} in the calculation [Fig. 8(f)] and is analogous to the totally symmetric ring-breathing mode of pyridine, which is the strongest feature in the pyridine NR spectrum.

The assignment of the modes in the NR spectrum below 950 cm^{-1} is more difficult, as most of the measured peaks are weak. However, it is possible to make a rough assignment (see Table I) to the intense peaks, namely those at 887, 870, 669, 640, and 488 cm^{-1}. The corresponding calculated peaks are at 900, 866, 675, 645, and 503 cm^{-1}, respectively.

Let us now consider the SER spectra in Fig. 3 and Table I. Both calculated and measured spectra in that figure are similar to the corresponding NR spectra in Fig. 2 (differing by an average of 8 cm^{-1}), so much of what we have already said about the NR spectra also applies to the comparison of theory and experiment in Fig. 3. The biggest differences in the measured spectra are in the widths of the peaks (all broader in SERS), and in the relative intensities of "doublets" at 1338 and 1314 cm^{-1}, 1244 and 1200 cm^{-1}. There are also some significant differences in the spectra below 900 cm^{-1}, with many more peaks appearing in the SER spectrum. The calculated spectra also show more lines below 900 cm^{-1} (though not as many as the experiment). The spectral assignments (Table I) show good agreement between theory and experiment for both SERS and NRS, but some of the measured SER lines were ignored in making these assignments.

We present Raman spectra as a function of orientation in Fig. 6. The most important trends in going from perpendicular to parallel to the surface are the intensity reduction in the peak at 1682 cm^{-1} and the enhancement of peaks at 1609, 1340, 900, and 503 cm^{-1}. This is not seen in the experiments, so we assume that the perpendicular orientation (or close thereto) is most appropriate.

C. Hyper-Raman spectra

The calculated bulk hyper-Raman spectrum is presented in Fig. 5, and the comparison of the measured and calculated

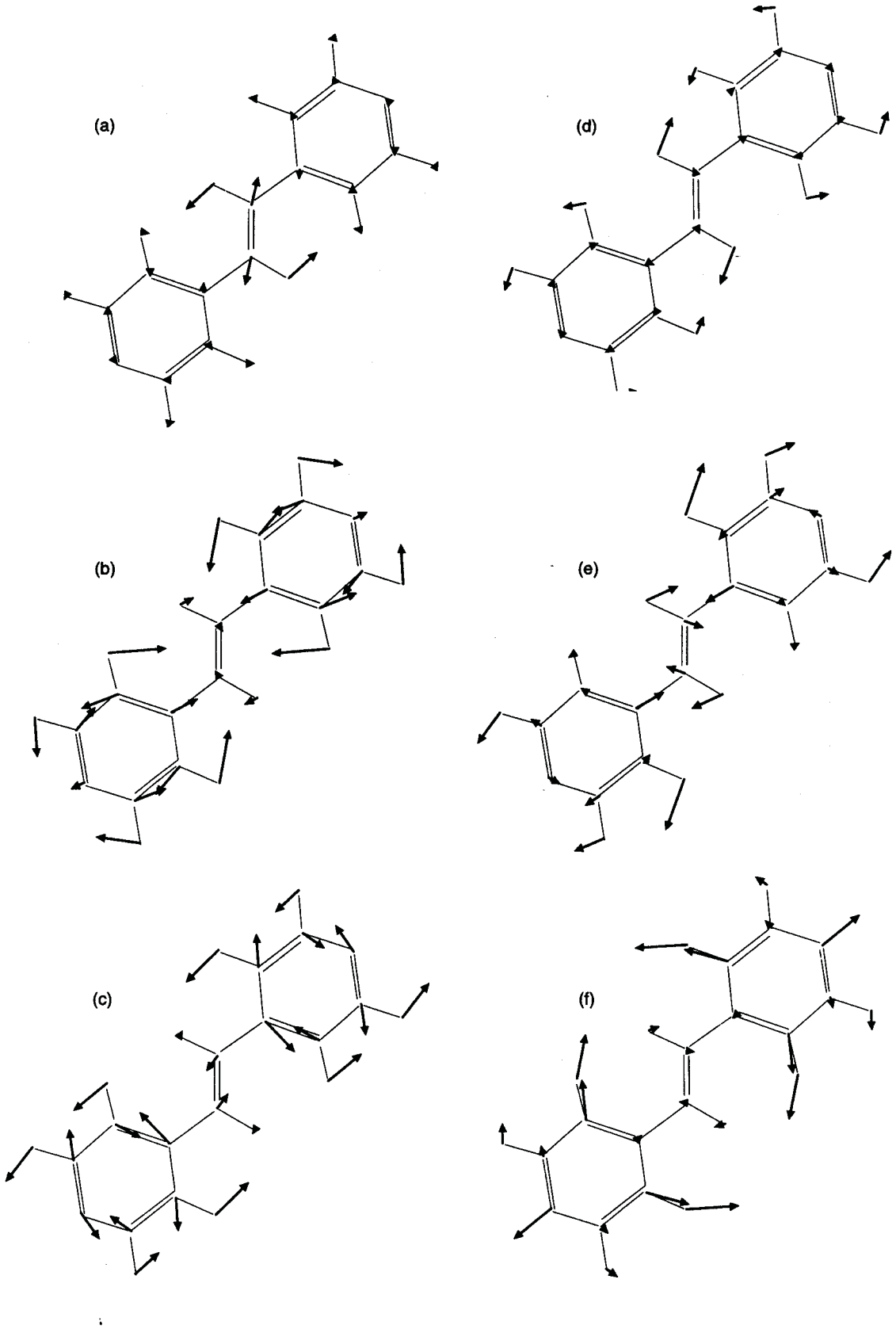

FIG. 8. Normal coordinates of BPE A_g modes as follows: (a) mode 1 (1682 cm^{-1}), (b) mode 2 (1609), (c) mode 3 (1560), (d) mode 6 (1363), (e), mode 9 (1201), and (f) mode 13 (986).

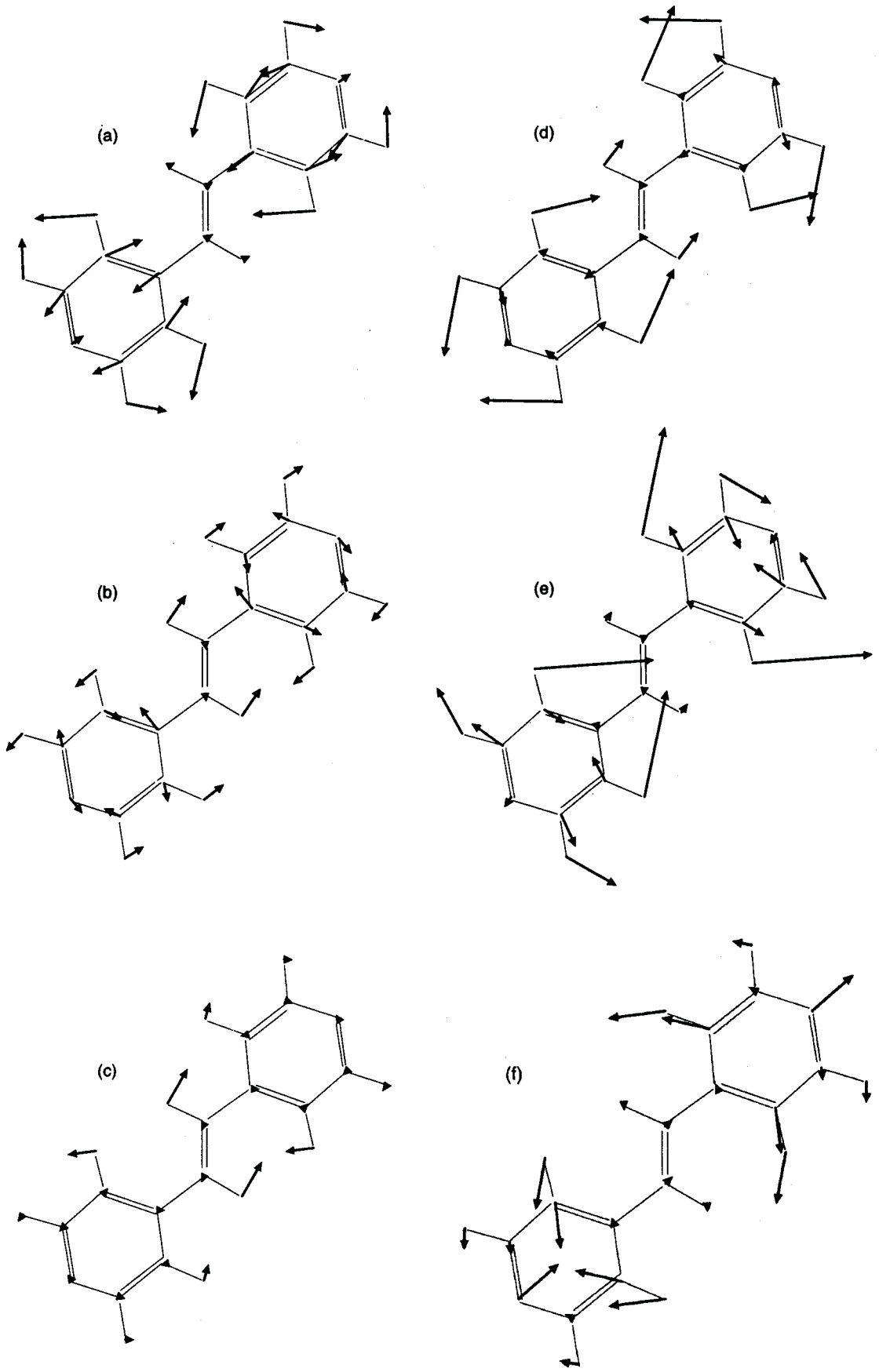

FIG. 9. Same as Fig. 8 but for B_u modes as follows: (a) mode 1 (1610 cm^{-1}), (b) mode 2 (1569), (c) mode 6 (1302), (d) mode 8 (1221), (e) mode 11 (1071), and (f) mode 12 (987).

SEHR spectra is shown in Fig. 4. The assignments are shown in Table I, and in this case we see that the measured and calculated intensities and frequencies do not match as well as for the IR or Raman spectra, with a 34 cm^{-1} average error for both symmetries. This increase in error is mostly due to a few assignments which are quite different from their IR counterparts (the 1289, 664, 599, and 552 cm^{-1} peaks). Obviously one of these assignments must be incorrect, but it is not obvious which. If these problem assignments are factored out, the average absolute difference between the SEHRS and IR lines is 10 cm^{-1} for B_u symmetry. The most intense band in the calculated and experimental SEHRS spectra is at 1610 cm^{-1}, and 1592 cm^{-1}, respectively, corresponding to pyridine ring stretching [Fig. 9(a)], and matching closely the most intense IR mode.

The peaks at 1569 cm^{-1} and 1504 cm^{-1} also match experiment closely, but the 1526 cm^{-1} and 1473 cm^{-1} peaks in the measured spectrum have no counterpart in the calculations. This result is surprising given that the corresponding SER spectrum shows such good correspondence with the calculations in this same spectral region with measured SERS peaks at 1544 cm^{-1} and 1493 cm^{-1}. In fact, we noted above that the two SERS active modes are paired with the two SEHRS active modes, suggesting that each spectrum should exhibit two peaks. One possible explanation for this unexpected result is that these particular modes involve considerable N-atom motion parallel to the surface [see Figs. 8(c) and 9(b)], more so than any other of the modes being considered above 1000 cm^{-1}. Such modes would therefore be leading candidates for exhibiting significant interaction with the surface, and if so then perhaps this would lead to mixing between the SERS and SEHRS active modes, leading to four peaks. What is unexplained here is why the SERS shows two peaks while the SEHRS shows four, however it should be noted that there is strong potential dependence to the spectra[8(b)] which means that the degree of interaction with the surface can be varied significantly.

The peaks at 1418, 1366, 1302 [Fig. 9(c)], 1239, 1221 [Fig. 9(d)], and 1137 cm^{-1} compare favorably with the measured SEHRS results, both with respect to frequency and intensity. Below that the assignments are not as certain, but there is at least a one-to-one correspondence for all but the weakest lines in the measured spectrum down to 500 cm^{-1}. One of the biggest sources of ambiguity in the assignment is the SEHRS peak at 1007 cm^{-1}, which seems to be in good correspondence with its counterpart in the SERS spectrum. Logically then, this peak should be associated with the calculated mode at 987 cm^{-1} [Fig. 9(f)] which is the counterpart of the SERS band at 986 cm^{-1} [Fig. 8(f)]. However, the predicted SEHRS intensity for the 987 cm^{-1} peak is low (Table I). From the point of view of intensities, a better assignment for this SEHRS peak is the 1071 cm^{-1} mode [Fig. 9(e)] as this has the strongest SEHRS intensity in this region of the spectrum.

We now consider the orientation effect. Figure 7 shows how the spectra vary with orientation as the latter varies from perpendicular to parallel to the surface. We note that the most intense mode for parallel geometries is at 1137 cm^{-1}, while the most intense mode for the other angles considered is at 1610 cm^{-1}. Comparison of these results with Fig. 4 suggests that the BPE cannot be parallel to the surface. However, some of the modes at frequencies lower than 1000 cm^{-1} that are not seen in the perpendicular geometry, are recovered as the molecule is tilted, so it seems likely that the distribution of orientation of angles allows some probability for the molecule to be tilted.

V. CONCLUSION

This paper presents a detailed analysis of the IR, Raman, and hyper-Raman spectra of BPE using *ab initio* methods that have previously been successful in explaining the spectra of pyridine and benzene. The comparison between theory and experiment is generally quite good, both with respect to frequency and intensities, and the comparison is of comparable quality for the IR and SER spectra, but less for the SEHR spectra. A key result is that almost all of the lines in the spectrum can be explained assuming that the molecular symmetry is C_{2h}, which means that the surface does not seriously perturb the centrosymmetric environment of BPE under these electrochemical conditions. We found that many of the modes come in pairs that are close in frequency but of opposite symmetry. This leads to peaks in the SERS and SEHRS spectra that have similar frequencies and intensities, which explains how a centrosymmetric molecule can have so many SERS and SEHRS peaks that appear to overlap. One mode does not show this pairing, namely the 1682 cm^{-1} A_g mode, and this is clearly seen only in the Raman spectra. The orientation dependence of the spectra was studied and it appears that most of the results are consistent with BPE being perpendicular to the surface.

ACKNOWLEDGMENTS

This research was supported by NSF Grant Nos. CHE-9016490, CHE-940078, and by the donors of the Petroleum Research Fund, administered by the American Chemical Society, under Grant No. 29507 AC6, 5.

[1] R. W. Terhune, P. D. Maker, and C. M. Savage, Phys. Rev. Lett. **14**, 681 (1965); D. J. Campbell and L. D. Ziegler, Chem. Phys. Lett. **201**, 159 (1993); J. P. Neddersen, S. A. Mounter, J. M. Bostick, and C. K. Johnson, J. Chem. Phys. **90**, 4719 (1989); Y. Tezuka, S. Shin, and M. Ishigame, Phys. Rev. B **49**, 9312 (1994).

[2] D. V. Murphy, K. U. Von Raben, R. K. Chang, and P. B. Dorain, Chem. Phys. Lett. **85**, 43 (1982).

[3] J. T. Golab, J. R. Sprague, K. T. Carron, G. C. Schatz, and R. P. Van Duyne, J. Chem. Phys. **88**, 7942 (1988).

[4] S. Nie, L. A. Lipscomb, S. Feng, and N.-T. Yu, Chem. Phys. Lett. **167**, 35 (1990); N. T. Yu, S. Nie, and L. A. Lipscomb, J. Raman Spectrosc. **21**, 797 (1990); L. A. Lipscomb, S. Nie, S. Feng, and N. T. Yu, Chem. Phys. Lett. **170**, 4577 (1990).

[5] (a) C. K. Johnson and S. A. Soper, J. Phys. Chem. **93**, 7281 (1989); (b) H. Kneipp, K. Kneipp, and F. Seifert, Chem. Phys. Lett. **212**, 374 (1993); (c) K. Kneipp, H. Kneipp, and F. Seifert, *ibid.* **233**, 519 (1995); (d) A. V. Baranov, Ya. S. Bobovich, and V. I. Petrov, Sov. Phys. Usp. **33**, 812 (1990).

[6] C. K. Chen, A. R. B. de Castro, and Y. R. Shen, Phys. Rev. Lett. **46**, 145 (1981); C. T. Boyd, Th. Rasing, J. R. R. Leite, and Y. R. Shen, Phys. Rev. B **30**, 519 (1984); E. J. Zeman and G. C. Schatz, J. Phys. Chem. **91**, 634 (1987).

[7] M. Moskovits, Rev. Mod. Phys. **57**, 783 (1985); H. Metiu and P. Das, Annu. Rev. Phys. Chem. **35**, 507 (1984); M. Kerker, Acct. Chem. Res. **17**, 271 (1984); G. C. Schatz, *ibid.* **17**, 370 (1984); H. Metiu, Prog. Surf. Sci. **17**, 153 (1984).
[8] (a) J. C. Hulteen, G. C. Schatz, and R. P. Van Duyne (in preparation); (b) J. C. Hulteen, G. C. Schatz, and R. P. Van Duyne (in preparation).
[9] R. P. Van Duyne, J. C. Hulteen, and D. A. Treichel, J. Chem. Phys. **99**, 2101 (1993).
[10] W.-H. Yang and G. C. Schatz, J. Chem. Phys. **97**, 3831 (1992).
[11] S. Califano, *Vibrational States* (Wiley, London, 1976).
[12] S. J. Cyvin, J. E. Rauch, and J. C. Decius, J. Chem. Phys. **43**, 4083 (1965).
[13] J. H. Christie and D. J. Lockwood, J. Chem. Phys. **54**, 1141 (1971).
[14] F. Mulder, G. Van Dijk, and C. Huiszoon, Mol. Phys. **38**, 577 (1979).
[15] GAUSSIAN 92, Revision C, M. J. Frisch, G. W. Trucks, M. Head-Gordon, P. M. W. Gill, M. W. Wong, J. B. Foresman, B. G. Johnson, H. B. Schlegel, M. A. Robb, E. S. Replogle, R. Gompert, J. L. Andres, K. Raghavachari, J. S. Binkley, C. Gonzalez, R. L. Martin, D. J. Fox, D. J. Defrees, J. Baker, J. J. P. Stewart, and J. A. Pople (Gaussian, Inc., Pittsburgh, PA, 1992).
[16] J. A. Pople, H. B. Schlegel, R. Krishnan, D. J. Defrees, J. S. Binkley, M. J. Frisch, and R. A. Whiteside, Int. J. Quantum Chem. Symp. **15**, 269 (1981).